analytical chemistry

pubs.acs.org/ac Article

Electrochemiluminescence Resonance Energy Transfer System Based on Silver Metal−Organic Frameworks as a Double-Amplified Emitter for Sensitive Detection of miRNA-107

Siyu Xiao, Xiaoyan Wang, Changping Yang, Yongjian Jiang, Shujun Zhen, Chengzhi Huang,* and Yuanfang Li*

Cite This: *Anal. Chem.* 2022, 94, 1178−1186 Read Online

ACCESS | Metrics & More | Article Recommendations | Supporting Information

ABSTRACT: As a class of electrochemiluminescence (ECL) enhancers, silver-based materials have broad application prospects. In this work, a novel silver metal−organic framework (AgMOF) was developed as a self-enhanced ECL emitter by one-step mixing and standing at room temperature. The AgMOF could produce strong and stable ECL emissions based on a double-amplification method, which originated from the aggregation-induced ECL emission of ligands and catalyzing $S_2O_8^{2-}$ to produce more $SO_4^{\bullet-}$ by silver. Moreover, an ECL resonance energy transfer (ECL-RET) biosensor with AgMOF as a donor and BHQ2 as an acceptor was fabricated by duplex-specific nuclease (DSN)-assisted target recycling amplification to detect miRNA-107. The biosensor exhibited a strong ECL-RET effect due to the higher ECL emission of the AgMOF and perfect match of spectra between the AgMOF and BHQ2. Upon the introduction of DSN and target miRNAs, the specific DNA−RNA binding and nuclease cleaving could trigger the detachment of BHQ2, resulting in an increased ECL signal of AgMOF. Benefiting from the ECL-RET and DSN-assisted target recycling amplification methods, this biosensor achieved a wide linear relationship range from 20 to 120 fM with a low limit of detection (4.33 fM). This research presents an effective emitter for self-enhanced ECL systems, which broadens the potential ECL applications of silver-based nanomaterials.

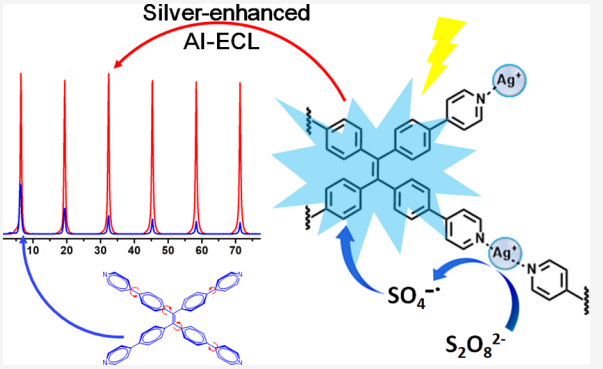

INTRODUCTION

Electrochemiluminescence (ECL) is a property by which emitters are oxidized or reduced to generate free radicals at the electrodes and to further create emissive excited-state products to emit light.[1−3] Most ECL systems have co-reactants added to the testing solution to obtain a relatively high emission.[4,5] Moreover, ECL enhancers which can facilitate the production of free groups can be used to enhance the ECL emission.[6−8] In particular, as a widely used co-reactant, peroxydisulfate can be catalyzed by silver-based materials to generate free radicals.[9,10] Silver which can facilitate the production of $SO_4^{\bullet-}$ has the potential to act as an ECL enhancer of the system, with peroxydisulfate as the co-reactant. However, silver may also cause the weakening of ECL emissions.[11,12] Therefore, it is important to develop a silver-based ECL luminophore which can be used as an enhancer while avoiding the quenching effect of silver for the development of an efficient ECL system.

Tetraphenylethen (TPE), as a kind of aggregation-induced emission (AIE) compound, has been studied extensively and has become the most attractive AIEgen due to its excellent properties, facile synthesis, and easy functionalization.[13−15] Interestingly, TPE also shows excellent aggregation-induced ECL (AI-ECL) property, that is, the supramolecular aggregates of TPE complexes displayed stronger ECL emissions than did their monomers.[16,17] In addition, the AI-ECL derivatives could effectively improve the ECL performance for some luminophores and show the potential to influence ECL by different types of substituents.[18,19] For instance, the AI-ECL emission is stronger for TPE derivatives with the nitro group compared to those with the amino group as a substituent.[20] TPE derivatives with different substituents can also be combined with different compounds flexibly to improve their own fluorescence emission efficiency.[21] Therefore, TPE derivatives as ECL emitters can exhibit relatively high emissions. However, when the organic compound was used as an ECL emitter, its ECL intensity will decrease sharply in the process of detection due to irreversible reactions, such as decomposition or oxidative polymerization.[22−25] Moreover, the too high excitation

Received: October 8, 2021
Accepted: December 23, 2021
Published: January 5, 2022

https://doi.org/10.1021/acs.analchem.1c04368
Anal. Chem. 2022, 94, 1178−1186

Scheme 1. (A) ECL Emission of TPPE and AgMOF and (B) Schematic Representation of the RET-ECL Biosensor Combined with DSN-Assisted Target Recycling Amplification for the Detection of miRNA-107

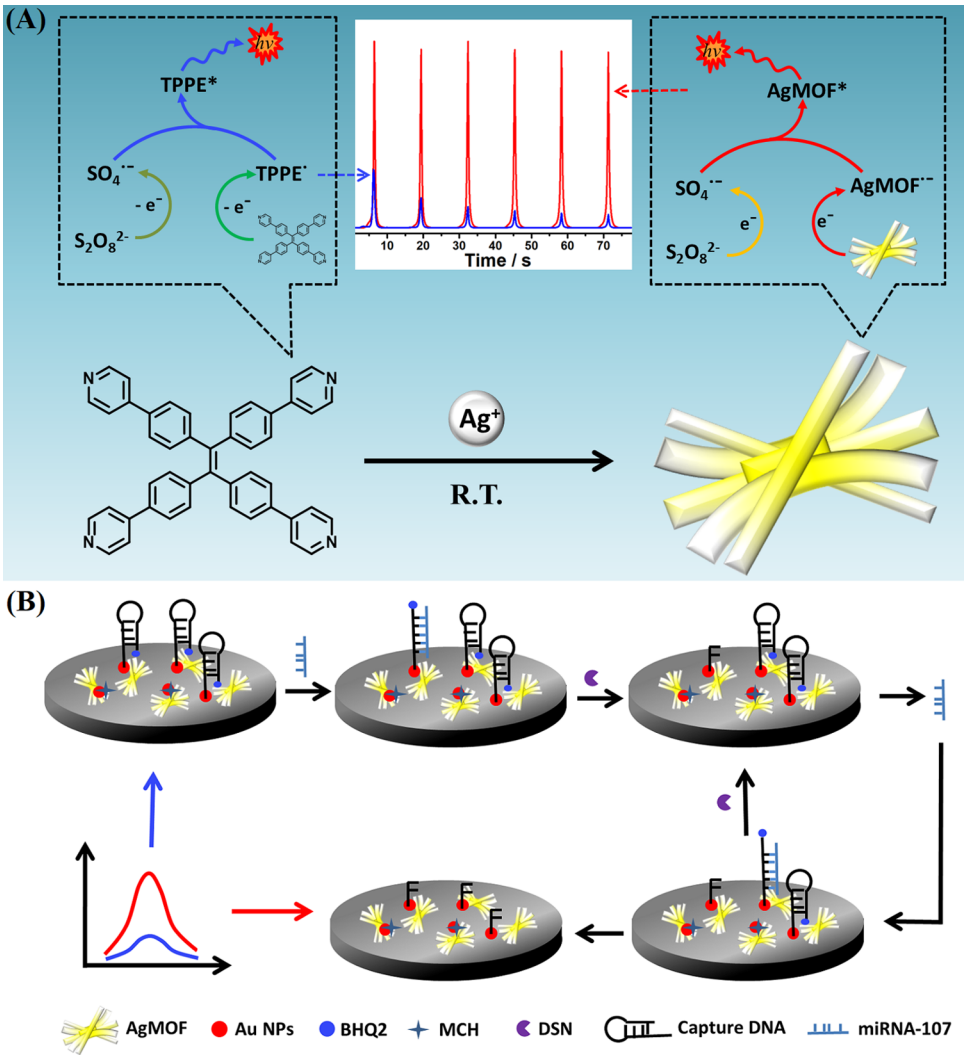

potential will damage the modified electrode and target, which greatly limits the practical application.[26,27] To obtain a relatively stable ECL emission, Li's group has established an effective way to increase the stability using metal organic polymers as ECL emitters.[25,28] Kim's group developed an ECL system with low excitation potential induced by the heavy atom effect.[29] Therefore, in order to solve the problems of unstable ECL emission and too high excitation potential, TPE derivatives and heavy metal ions are used to construct metal−organic frameworks (MOFs) as ECL emitters.

MOFs can be fine-tuned to exhibit unique properties by a careful design of the metallic units and organic linkers.[30] In particular, MOFs have been used to rigidify the AIEgens, where the excited-state nonradiative transition caused by intramolecular rotations was limited, resulting in intense luminescence.[31−33] At the same time, due to their permanent porosity and ultrahigh specific surface area, MOFs can significantly improve the carrying capacity of the luminescent groups and increase the reaction rate of luminophores and co-reactants and have received more and more attention as emitters, catalysts, and carriers in the ECL field.[34−37] Moreover, the composition of metal ions and organic ligands is rigid and directional in MOFs, which can avoid the adverse effects of metal ions on the luminescent center of the organic ligands.[38] Nowadays, some organic compounds with AI-ECL properties have been used as ligands to construct MOFs.[39,40]

Herein, 1,1,2,2-tetrakis(4-(pyridin-4-yl)phenyl)-ethene (TPPE), a kind of AI-ECL molecule, was assembled with silver-ion nodes to form a novel silver metal−organic framework (AgMOF) (Scheme 1A). Compared with the ligand TPPE, the ECL emission of AgMOF had been more stable and stronger. The stronger ECL emission was attributed to the AI-ECL emission of TPPE and the self-enhanced catalysis of $S_2O_8^{2-}$ to produce more $SO_4^{\bullet-}$. In addition, the more stable ECL emission was due to TPPE being made into MOFs. Furthermore, in order to expand the application research of AI-ECL, combined with duplex-specific nuclease (DSN)-assisted target recycling amplification, we proposed a ECL resonance energy transfer (ECL-RET) strategy to fabricate biosensors (Scheme 1B) with AgMOF as a donor and BHQ2 as an acceptor to sensitively detect target miRNA-107. The concentration of miRNA-107 was associated with a variety of diseases.[41] As a cancer marker, miRNA-107 which is expressed in a variety of cancers was selected as the target.[42] For example, miRNA-107 was involved in hepatitis C virus-mediated induction of inflammatory responses and fibrosis.[43]

https://doi.org/10.1021/acs.analchem.1c04368
Anal. Chem. 2022, 94, 1178−1186

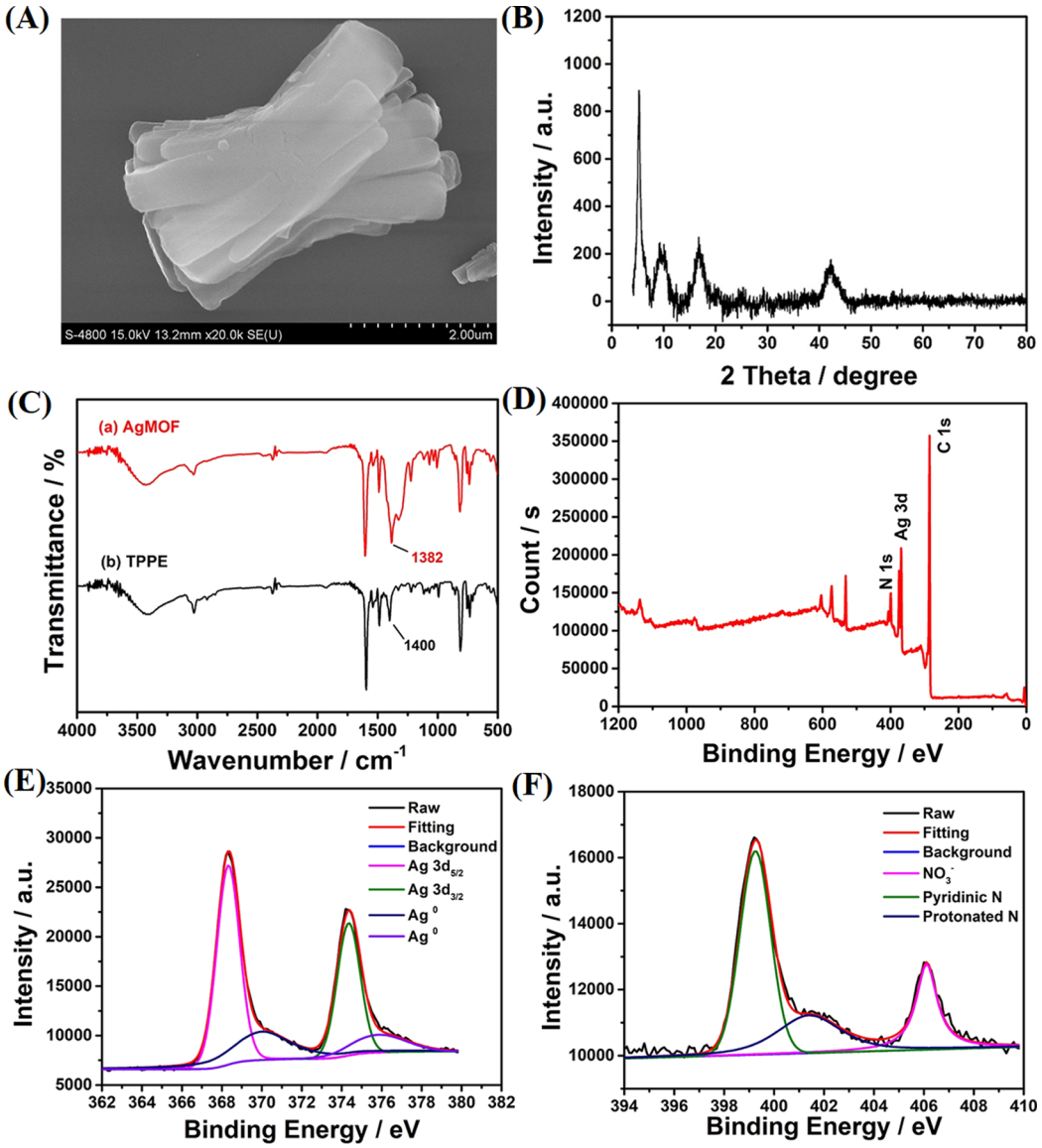

Figure 1. (A) SEM image of AgMOF. (B) XRD pattern of AgMOF. (C) FTIR spectra of AgMOF and TPPE. (D) XPS spectrum of AgMOF. (E) High-resolution XPS spectra of Ag. (F) High-resolution XPS spectra of N.

Therefore, miRNA-107 could be used as a biomarker of various diseases, and it was important to detect miRNA-107 for the diagnosis and treatment of the initial stage of a variety of diseases. Benefiting from the strong ECL emission of AgMOF, ECL-RET, and DSN-assisted target recycling amplification, the designed ECL biosensor showed high sensitivity and selectivity for miRNA-107 detection.

EXPERIMENTAL SECTION

Reagents and Apparatus. The reagents and apparatus details are provided in the Supporting Information. The nucleic acid sequence is shown in Table S1.

Preparation of AgMOF. In the preparation of AgMOF, 18 mg of TPPE was dissolved in 6 mL of DMF, and 19.1 mg of $AgNO_3$ was dissolved in 3 mL of water. Then, 800 μL of the TPPE solution and 200 μL of $AgNO_3$ solution were added into a 2 mL Eppendorf tube. After mixing, the mixture was allowed to stand for 24 h at room temperature. The resulting AgMOF was washed twice with DMF and water, respectively, and then collected by a centrifuge operated at 8000 rpm for 3 min. For further experiments, the AgMOF was dried to remove the solvent by freeze-drying treatment.

Preparation of ECL Sensor. A glassy carbon electrode (GCE) was polished with 0.3 and 0.05 μm alumina powder to obtain a mirror-like surface. Then, the GCE was rinsed with ethanol and water and dried with purified nitrogen streams. Subsequently, 5 μL of the dried AgMOF dispersion solution (1 mg/mL) was cast on the surface of a clean GCE and dried at room temperature.

Construction of the Biosensor and Analysis Procedure. The ECL-RET biosensor with DSN enzyme-assisted amplification was constructed as follows: hairpin-capture DNA (cDNA) was annealed by heating at 95 °C for 3 min and slowly cooling to 25 °C. Then, 5 μL of AgMOF and 5 μL of Au NP solution were dropped onto the GCE surface and dried naturally, respectively. Next, 5 μL of 2 μM thiolated cDNA was dropped onto the modified GCE and incubated overnight, and 6-mercapto-1-hexanol (MCH) was used to block the nonspecific sites for 1 h. Subsequently, 5 μL of miRNA-107 and 0.2 U DSN were added to the modified GCE and incubated

https://doi.org/10.1021/acs.analchem.1c04368
Anal. Chem. 2022, 94, 1178−1186

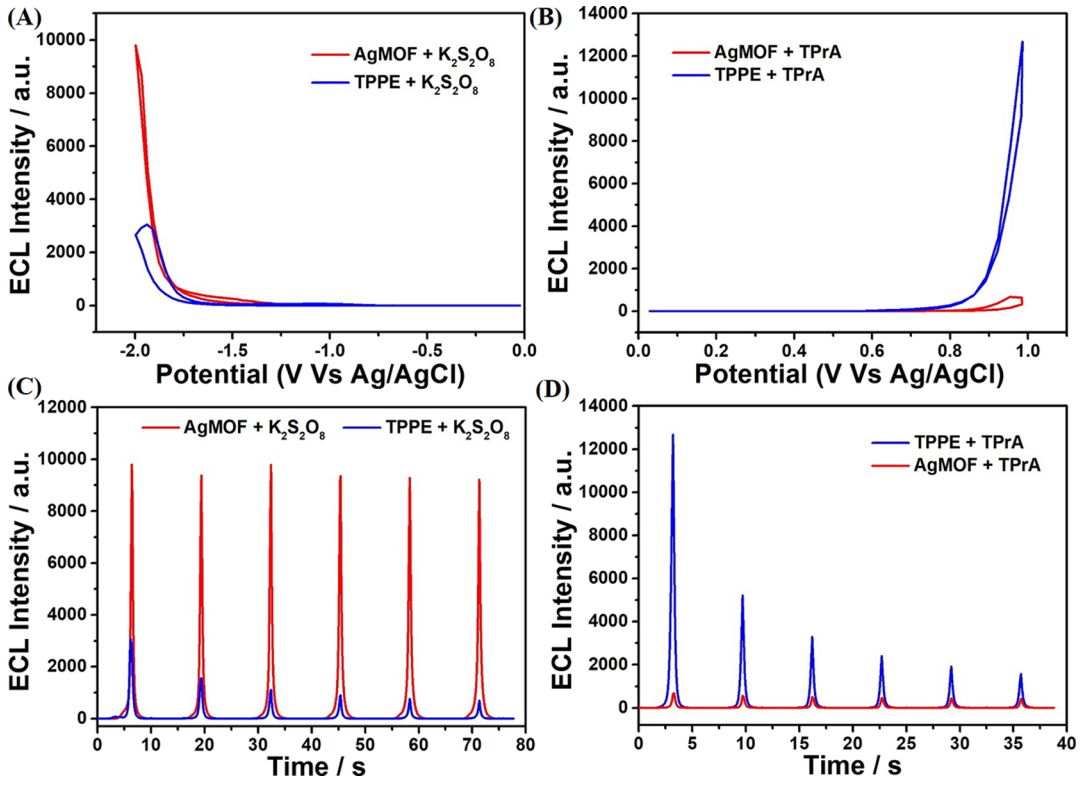

Figure 2. (A) Cathodic ECL emission of TPPE and AgMOF with $K_2S_2O_8$ as a co-reactant. (B) Anodic ECL emission of TPPE and AgMOF with tri-*N*-propylamine as the co-reactant. (C) ECL emission curve of TPPE and AgMOF at the cathode. (D) ECL emission curve of TPPE and AgMOF at the anode.

for 2 h at 50 °C. DSN-assisted miRNA recycling amplification was performed in the 50 mM Tris−HCl (pH 8.0) buffer containing 10 mM $MgCl_2$. Next, the residual fragments of DNA and detached BHQ2 were washed by ultrapure water. The modified GCE was tested in the electrolyte of the 0.1 M pH 7.4 phosphate-buffered solution (PBS) with 70 mM $K_2S_2O_8$ for measurements. The voltage of the photomultiplier tube was set at 800 V.

Human Sample Detection. Plasma was collected by a centrifuge at 3000 rpm, 3 min. Then, protein in plasma was removed by ultrafiltration. The standard sample of miRNA-107 was added to the serum sample for testing. Each spiked serum sample will be calibrated with a blank sample.

RESULTS AND DISCUSSION

Synthesis and Characterization of AgMOF. TPPE as the ligand could form MOFs with silver clusters, but the method was relatively complicated, not only time-consuming but also involving the use of a variety of toxic reagents.[44] In this work, the ligand TPPE and silver ions were simply mixed and allowed to stand overnight to obtain AgMOF. Moreover, the morphology of AgMOF was changed by adjusting the volume ratio of the solvent DMF to water (Figure S1). In the process of synthesizing AgMOFs, the concentration of TPPE is constant. The volume of DMF was reduced and that of water was increased to make the total volume of the mixed solvent 1 mL. At the same time, the ratio of the amount of the ligand TPPE and the silver ion is 1:2. As the volume of water gradually increases, the size of AgMOF becomes larger, and the morphology becomes more regular, showing as microflowers. Unless otherwise indicated, the AgMOF used for characterization and in all the electrochemical experimental part had the volume ratio of DMF:H_2O = 4:1.

Scanning electron microscopy (SEM) showed that AgMOF was a collection of many elongated flake crystals (Figure 1A). The middle of AgMOF was fused together, and the two ends were scattered in a flower-like shape. The X-ray diffraction (XRD) patterns showed AgMOF with clear XRD diffraction peaks, which proved that AgMOF had a crystal structure (Figure 1B). The Fourier transform infrared (FTIR) spectra (Figure 1C) showed that the red shift of 18 cm^{-1} might be caused by the coordination of the metal ion to the N atom.[45] X-ray photoelectron spectroscopy (XPS) was used to reveal the elemental composition and chemical state of AgMOF. XPS showed obvious peaks of Ag 3d, C 1s, and N 1s, indicating that these elements are abundant in AgMOFs (Figure 1D). The high-resolution XPS spectrum of silver (Figure 1E) showed that the peaks of Ag $3d_{3/2}$ (374.7 eV) and Ag $3d_{5/2}$ (368.7 eV) corresponded to the peaks of Ag^+, while the peaks at 376.0 and 370.0 eV proved the existence of Ag^0 species in the samples.[46−48] It indicated that silver ions as the nodes in the AgMOF and silver clusters may also be formed as the nodes of the AgMOF. The high-resolution XPS spectrum of N 1s (Figure 1F) showed that the peaks at 399.3, 401.5, and 406.1 eV belonged to pyridine, protonated pyridine, and nitrate ion, respectively.[49,50] The protonated pyridine indicated that the pyridyl group is coordinated to silver in the AgMOF.

ECL Performance of AgMOF. With peroxydisulfate as a co-reactant, both TPPE and AgMOF could produce cathode ECL emission, and the ECL emission of AgMOF was stronger (Figure 2A). As a double-amplified emitter, the strong ECL emissions of AgMOF come from the aggregation of TPPE and the enhancement of silver. The ECL emission of TPPE with

https://doi.org/10.1021/acs.analchem.1c04368
Anal. Chem. 2022, 94, 1178−1186

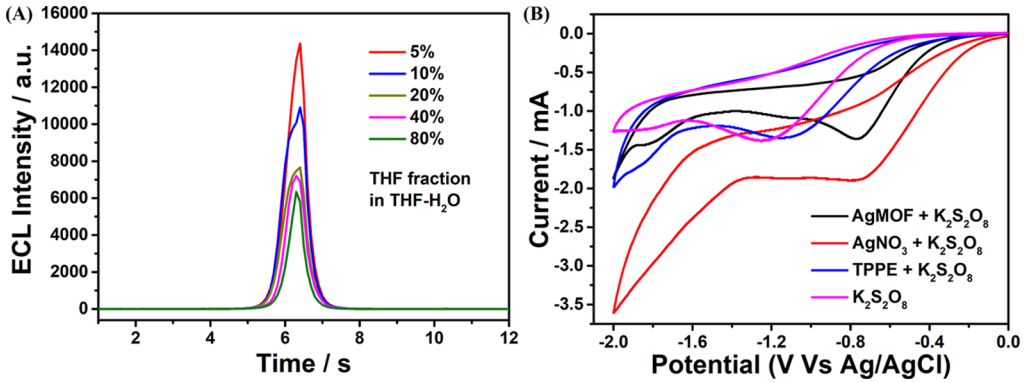

Figure 3. (A) AI-ECL behavior and ECL intensity changes of TPPE upon variation of the THF fraction of a THF−H_2O mixture solution. (B) Cyclic voltammetry (CV) curves for $K_2S_2O_8$ alone (pink line), and the CV curves for TPPE (blue line), $AgNO_3$ (red line), and AgMOF (black line), with $K_2S_2O_8$ in 0.1 M PBS.

AI-ECL properties would increase as the degree of aggregation increases, while the state of TPPE in AgMOF becomes orderly concentrated.[16] On the other hand, silver could accelerate the electrochemical reduction of peroxydisulfate and enhance the ECL intensity of the system with peroxydisulfate as the co-reactant.[9] With tri-*N*-propylamine as the co-reactant, TPPE could produce strong anode ECL emission, while AgMOF hardly produced ECL emission (Figure 2B). The possible reason was that the optimal excitation potential of AgMOF at the anode had changed, and the co-reactant was no longer tri-*N*-propylamine. Moreover, the cathode ECL emission of TPPE was significantly attenuated during the cycle, while AgMOF could produce a relatively stable ECL emission (Figure 2C). The anode ECL emission of TPPE had also been significantly attenuated during the cycle (Figure 2D).

When the scanning potential was between 0 and 1.5 V, AgMOF could produce a strong anode ECL emission, but TPPE could not produce ECL emission with NaClO as the co-reactant (Figure S2A). When the scanning potential was between 0 and 2.0 V, the optimal excitation potential of TPPE was about 1.1 V with tri-*N*-propylamine as the co-reactant, and the optimal excitation potential of AgMOF was about 1.6 V with NaClO as the co-reactant, respectively (Figure S2B). The optimal excitation potential and the co-reactant of the luminophore changed after the formation of AgMOF. The possible reason was that silver changes the electron cloud density of TPPE and further changes the optimal excitation potential.[18,20,29] The ECL emission of TPPE and AgMOF with tri-*N*-propylamine and NaClO as co-reactants was tested in the range of 0−2.0 V, respectively (Figure S2C). TPPE produced strong ECL emission only in the first cycle, and there was almost no ECL emission in the following four cycles. However, TPPE could produce strong and slowly decayed ECL emissions in the range of 0−1.0 V (Figure 2D). This indicated that the high potential was detrimental to the ECL emission of TPPE. The possible reason was that too high potential will destroy the structure of the organic light-emitting species.[26,27] Moreover, AgMOF showed strong ECL emission in five cycles, so an effective method to protect the organic light-emitting species is incorporating it into a MOF. Unfortunately, the ECL emission of AgMOF was strong but not stable at the optimal excitation potential (Figure S2D).

From the observed behavior above, it can be concluded that AgMOF could produce both cathode and anode ECL emissions. However, it is disadvantageous for fabricating biosensors due to the unstable anode ECL emission. Therefore, we used AgMOF as the cathode ECL emitter to fabricate the biosensor.

ECL Mechanism. To demonstrate the AI-ECL property of TPPE, we dispersed TPPE in tetrahydrofuran−water (THF−H_2O) mixture solvents with different volume ratios to make TPPE have different aggregation states through self-assembly. As shown in Figure S3, there was almost no fluorescence emission when there was too much THF in the mixed solvent (Figure S3a,b). When the volume of THF in the mixed solvent decreased, the fluorescence of TPPE became stronger (from Figure S3c,e). This was the performance of a typical compound with AIE properties.[17,51] Therefore, TPPE has different aggregation states in the THF−H_2O mixture solvents with different volume ratios. Furthermore, five different TPPE with different aggregation states were modified on the GCE and dried at room temperature. Then, we measured the ECL of the five different TPPE in PBS as the supporting electrolyte containing 70 mM $K_2S_2O_8$ as the co-reactant (Figure 3A). The ECL intensity of TPPE increased significantly when the THF fraction decreased from 80 to 5% in the mixed solvent. This indicated that TPPE had an obvious AI-ECL behavior, which is in agreement with the results of the fluorescence of TPPE.[16,39] The ECL intensity of TPPE was relatively high when the fraction of THF was 80 and 40%. This was because the degree of aggregation of TPPE increased during the drying process on the electrode at room temperature.

For investigating the ECL enhancement mechanism of silver, we compared the CV curves of bare GCE, TPPE, $AgNO_3$, and AgMOF in $K_2S_2O_8$ solution (Figure 3B). The CV reduction peak of $K_2S_2O_8$ was at −1.2 V, which means $S_2O_8^{2-}$ was electrochemically reduced to $SO_4^{\bullet-}$. The CV reduction peak of AgMOF in $K_2S_2O_8$ solution was at −0.8 V, and this peak belongs to the electrochemical reduction of $K_2S_2O_8$. After mixing AgMOF and $K_2S_2O_8$, the CV peak of $S_2O_8^{2-}$ that reduced to $SO_4^{\bullet-}$ changed from −1.2 to −0.8 V, indicating that $S_2O_8^{2-}$ was easier to be reduced to $SO_4^{\bullet-}$. The CV peak of $S_2O_8^{2-}$ that reduced to $SO_4^{\bullet-}$ changed from −1.2 to −0.8 V after mixing with $AgNO_3$, which had been reported earlier.[9] Therefore, the possible enhancement mechanism was that AgMOF could effectively accelerate the generation of $SO_4^{\bullet-}$.[52] The reduced CV peak of $S_2O_8^{2-}$ did not chang after mixing TPPE, suggesting that silver of AgMOF was considered as a catalytically active center.

https://doi.org/10.1021/acs.analchem.1c04368
Anal. Chem. 2022, 94, 1178−1186

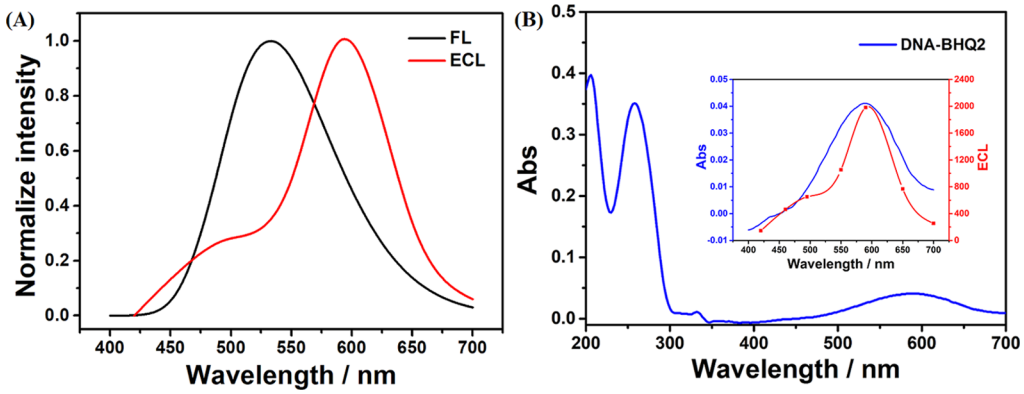

Figure 4. (A) Fluorescence spectrum (black line) and ECL spectrum (red line) of AgMOF. (B) UV−vis absorption spectrum of cDNA−BHQ2, and the inset shows the overlap between the ECL emission spectrum of AgMOF and the UV−vis absorption spectrum of BHQ2.

From the above, it is observed that TPPE is a molecule with AI-ECL properties. After the formation of AgMOF, the ECL emission of AgMOF was stronger than that of TPPE. The strong ECL emission of AgMOF was attributed to the AI-ECL properties of TPPE.[39,40] On the other hand, silver of AgMOF was considered as a catalytically active center to accelerate the generation of $SO_4^{\bullet-}$ and enhance the ECL emission of AgMOF.[9,52] Thus, the possible ECL mechanism was proposed. Briefly, the AgMOF and $K_2S_2O_8$ were electrochemically reduced to $AgMOF^{\bullet-}$ and $SO_4^{\bullet-}$, respectively. Meanwhile, the AgMOF could accelerate the reduction of $S_2O_8^{2-}$ to generate more $SO_4^{\bullet-}$. Then, the $AgMOF^{\bullet-}$ reacted with $SO_4^{\bullet-}$ further to produce AgMOF* as the light-emitting species. Moreover, the AI-ECL characteristics of TPPE would further enhance the ECL emission of AgMOF. The possible ECL mechanism is listed as follows

$$S_2O_8^{2-} + e^- \xrightarrow{\text{AgMOF}} SO_4^{2-} + SO_4^{\bullet-} \quad (1)$$

$$\text{AgMOF} + e^- \rightarrow \text{AgMOF}^{\bullet-} \quad (2)$$

$$SO_4^{\bullet-} + \text{AgMOF}^{\bullet-} \rightarrow SO_4^{2-} + \text{AgMOF}^* \quad (3)$$

$$\text{AgMOF}^* \rightarrow \text{AgMOF} + h\nu \quad (4)$$

Fabrication of the ECL Biosensor. To expand the analysis application of the system, combined with DSN-assisted target recycling amplification, the ECL-RET biosensor was fabricated with AgMOF as the donor and BHQ2 as the acceptor. The fluorescence and the ECL spectrum of AgMOF are shown in Figure 4A. The maximum fluorescence intensity and the maximum ECL intensity of AgMOF were at 525 and 600 nm, respectively. Then, the UV−vis absorption spectrum of cDNA was measured (Figure 4B). The absorption of 200−300 nm belonged to DNA, and the absorption of 400−700 nm belonged to BHQ2. There was a good overlap between the ECL emission spectrum of AgMOF and the UV−vis absorption spectrum of BHQ2, indicating that there may be an ECL-RET between the AgMOF and BHQ2 (Figure 4B, inset).

The assembly process of the ECL biosensor was characterized via electrochemical impedance spectroscopy (EIS). As shown in Figure 5, the bare GCE exhibits a semicircle domain, which indicated the mass-transfer process (curve a). A little bigger arch than bare GCE was shown distinctly after the AgMOF was modified on the electrode, indicating that the electron-transfer resistance increased (curve b). When AuNPs were connected to the surface of the AgMOF, the arch became bigger (curve c). After reacting with cDNA, the electron-transfer resistance increased (curve d). When MCH was connected to the surface of the electrode, the charge-transfer resistance further increased (curve e). There was a corresponding relationship between the change of the impedance value of the electrode and the assembly process of the biosensor, indicating that the electrode assembly was successful.

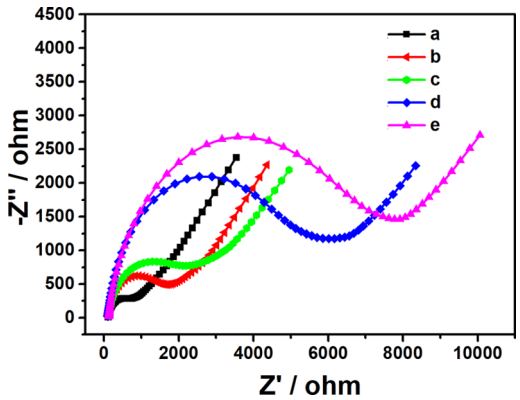

Figure 5. EIS curves of (a) bare GCE, (b) AgMOF/GCE, (c) AuNPs/AgMOF/GCE, (d) cDNA/AuNPs/AgMOF/GCE, and (e) MCH/cDNA/AuNPs/AgMOF/GCE in 5.0 mM $[Fe(CN)_6]^{3-/4-}$.

Analytical Ability of the ECL-RET Biosensor. To obtain favorable detection results, several interrelated factors were optimized, including the different AgMOFs, the concentration of AgMOFs, $K_2S_2O_8$, and pH. Five AgMOFs with different morphologies were synthesized using different volume ratios of DMF and water. The ECL emissions of five different AgMOFs were tested under the same conditions (Figure S4A). The results showed that the volume ratio of DMF and water with the maximum ECL intensity of AgMOF was 4:1. The best concentration of AgMOF was 1.0 mg/mL (Figure S4B). The suitable concentration of $K_2S_2O_8$ was 70 mM (Figure S4C). The excellent pH of PBS was 7.2 (Figure S4D).

In the ECL biosensor, the cDNA−BHQ2-modified AgMOF electrode exhibited a strong ECL-RET effect due to the higher ECL emission of the donor and perfect match of the spectra. cDNA with the hairpin structure and BHQ2 which was near the AgMOF weaken the ECL emission of AgMOF due to ECL-RET. When target miRNA-107 was present, the hairpin structure of cDNA would be opened, and a DNA−RNA hybrid

https://doi.org/10.1021/acs.analchem.1c04368
Anal. Chem. 2022, 94, 1178−1186

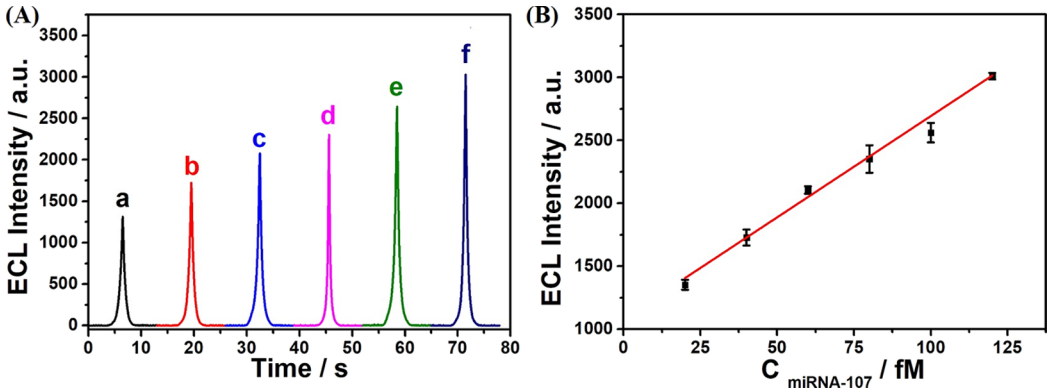

Figure 6. (A) ECL response of the biosensor to various concentrations of target miRNA-107 (a–f: 20, 40, 60, 80, 100, and 120 fM). (B) Calibration plots between the ECL intensity and the concentrations of miRNA-107.

chain would be formed with miRNA-107. Then, cDNA in the DNA–RNA hybrid chain would be cut by the DSN enzyme, and miRNA-107 would be released to combine with another cDNA and enter the next cycle. BHQ2 on cDNA was released. Therefore, the ECL-RET between BHQ2 and AgMOF was disrupted, and the ECL emission of the AgMOF was restored. Under optimal conditions, the ECL intensity of the biosensor gradually increased with the increased concentration of miRNA-107, indicating that the biosensor could be employed to quantify miRNA-107 (Figure 5A). There was a good relationship between the ECL intensity and miRNA-107 concentration in the range from 20 to 120 fM. Further, the linear regression equation was described as $I = 1084.4 + 16.1c$, where c symbolized the miRNA-107 concentration and $R^2 = 0.993$ (Figure 6B). The limit of detection was calculated to be 4.33 fM by the ratio of 3σ to K, where σ was the standard deviation of the blank measurements ($n = 10$), and K was the slope of the corresponding linear regression equation.

Stability is important to the obtained ECL biosensor. The stability of the biosensor was investigated under consecutive scanning for nine cycles with determination of 100 fM mRNA-107 (Figure S5). These responses almost remained constant with RSDs of 2.42%.

The selectivity of the ECL-RET biosensor for miRNA-107 (100 fM) was surveyed in the blank assay and other controlled miRNA sequences of 1 pM for miRNA-21 and miRNA-141, showing that the most changes in the ECL intensity of the analyte was of miRNA-107 (Figure S6).

Human blood samples were obtained from three volunteers supported by the institutional committee of Southwest University. All the samples from the volunteers were used only in this experiment. The quantitation of miRNA-107 was approved by all volunteers, and informed consent was obtained. All experimental procedures were performed in accordance with the relevant laws and the institutional guidelines of ethical standards of the Institutional Committee of Southwest University (approval number, yxy202112), and all the guidelines were followed throughout the present study. The sample analysis experimental protocol was approved by the Institutional Committee of Southwest University (approval number, yxy202112). As shown in Table S2, the ECL-RET biosensor was further used to quantify miRNA-107 in the human blood serum sample to illustrate that the biosensor had potential application in the analysis of real samples.

CONCLUSIONS

In conclusion, a novel AgMOF as the ECL emitter with double amplification was designed, and the ECL-RET biosensor based on AgMOF as the donor and BHQ2 as the acceptor was established. The novel AgMOF could produce a stronger and stable ECL emission at the cathode. The enhancement mechanism of AgMOF was ascribed to the AI-ECL emission of TPPE and to the self-enhanced catalysis of $S_2O_8^{2-}$ to produce more $SO_4^{\bullet -}$. In addition, a more stable ECL emission could be produced by incorporating organic light-emitting species into MOFs. Further, a biosensor based on ECL-RET was constructed to detect miRNA-107 with desirable high sensitivity and selectivity. This high sensitivity of the biosensor was ascribed to the (1) high ECL-RET efficiency between the strong ECL emission of the AgMOF donor and the BHQ2 acceptor and (2) DSN-assisted target recycling amplification. This work broadens the application of silver-based nanomaterials as self-enhanced ECL emitters, holding promise for potential applications in various types of nucleic acid detection.

ASSOCIATED CONTENT

Supporting Information

The Supporting Information is available free of charge at https://pubs.acs.org/doi/10.1021/acs.analchem.1c04368.

Reagents and apparatus; characterization of the AgMOF; ECL behavior of the AgMOF; EIS characterization of the biosensor; optimization experiment; selectivity of the biosensor; sequences of nucleic acids; and real blood sample analysis (PDF)

AUTHOR INFORMATION

Corresponding Authors

Chengzhi Huang – *Key Laboratory of Luminescent and Real-Time Analytical System (Southwest University), Chongqing Science and Technology Bureau, College of Pharmaceutical Sciences, Southwest University, Chongqing 400715, P. R. China*; orcid.org/0000-0002-1260-5934; Email: liyf@swu.edu.cn

Yuanfang Li – *Key Laboratory of Luminescence Analysis and Molecular Sensing (Southwest University), Ministry of Education, College of Chemistry and Chemical Engineering, Southwest University, Chongqing 400715, P. R. China*; orcid.org/0000-0001-5710-4423; Email: chengzhi@swu.edu.cn

https://doi.org/10.1021/acs.analchem.1c04368
Anal. Chem. 2022, 94, 1178–1186

Authors

Siyu Xiao − *Key Laboratory of Luminescence Analysis and Molecular Sensing (Southwest University), Ministry of Education, College of Chemistry and Chemical Engineering, Southwest University, Chongqing 400715, P. R. China*

Xiaoyan Wang − *Key Laboratory of Luminescence Analysis and Molecular Sensing (Southwest University), Ministry of Education, College of Chemistry and Chemical Engineering, Southwest University, Chongqing 400715, P. R. China*

Changping Yang − *Key Laboratory of Luminescence Analysis and Molecular Sensing (Southwest University), Ministry of Education, College of Chemistry and Chemical Engineering, Southwest University, Chongqing 400715, P. R. China*

Yongjian Jiang − *Key Laboratory of Luminescent and Real-Time Analytical System (Southwest University), Chongqing Science and Technology Bureau, College of Pharmaceutical Sciences, Southwest University, Chongqing 400715, P. R. China;* orcid.org/0000-0003-4652-4689

Shujun Zhen − *Key Laboratory of Luminescence Analysis and Molecular Sensing (Southwest University), Ministry of Education, College of Chemistry and Chemical Engineering, Southwest University, Chongqing 400715, P. R. China;* orcid.org/0000-0003-1236-5501

Complete contact information is available at: https://pubs.acs.org/10.1021/acs.analchem.1c04368

Notes

The authors declare no competing financial interest.

■ ACKNOWLEDGMENTS

This work was financially supported by the National Natural Science Foundation of China (NSFC, no. 21874109) and the Chongqing Talents Program for Outstanding Scientists (No.cstc2021ycjh-bgzxm0179).

■ REFERENCES

(1) Ding, Z.; Quinn, B. M.; Haram, S. K.; Pell, L. E.; Korgel, B. A.; Bard, A. J. *Science* **2002**, *296*, 1293.

(2) Guo, W.; Ding, H.; Gu, C.; Liu, Y.; Jiang, X.; Su, B.; Shao, Y. *J. Am. Chem. Soc.* **2018**, *140*, 15904−15915.

(3) Wong, J. M.; Zhang, R.; Xie, P.; Yang, L.; Zhang, M.; Zhou, R.; Wang, R.; Shen, Y.; Yang, B.; Wang, H. B.; Ding, Z. *Angew. Chem., Int. Ed.* **2020**, *59*, 17461−17466.

(4) Tan, X.; Zhang, B.; Zou, G. *J. Am. Chem. Soc.* **2017**, *139*, 8772−8776.

(5) Zinna, F.; Voci, S.; Arrico, L.; Brun, E.; Homberg, A.; Bouffier, L.; Funaioli, T.; Lacour, J.; Sojic, N.; Di Bari, L. *Angew. Chem., Int. Ed.* **2019**, *58*, 6952−6956.

(6) Xiao, S. Y.; Zhen, S. J.; Huang, C. Z.; Li, Y. F. *Biosens. Bioelectron.* **2021**, *186*, 113263.

(7) Khoshfetrat, S. M.; Khoshsafar, H.; Afkhami, A.; Mehrgardi, M. A.; Bagheri, H. *Anal. Chem.* **2019**, *91*, 6383−6390.

(8) Mo, G.; Qin, D.; Jiang, X.; Zheng, X.; Mo, W.; Deng, B. *Sens. Actuators, B* **2020**, *310*, 127852.

(9) Xiao, S. Y.; Li, Y.; Zhen, S. J.; Huang, C. Z.; Li, Y. F. *Electrochim. Acta* **2020**, *357*, 136842.

(10) Fang, Q.; Lin, Z.; Lu, F.; Chen, Y.; Huang, X.; Gao, W. *Electrochim. Acta* **2019**, *302*, 207−215.

(11) Ai, Z.; Zhao, M.; Han, D.; Chen, K.; Xiong, D.; Tang, H. *Biosens. Bioelectron.* **2021**, *179*, 113059.

(12) Ali, A.; Zhao, J.; Khan, M. S.; Wang, H.; Ren, X.; Hu, L.; Manzoor, R.; Wu, D.; Wei, Q. *Sens. Actuators, B* **2021**, *329*, 129155.

(13) Zhao, Z.; Lam, J. W. Y.; Tang, B. Z. *J. Mater. Chem.* **2012**, *22*, 23726−23740.

(14) Huang, J.; Yang, X.; Li, X.; Chen, P.; Tang, R.; Li, F.; Lu, P.; Ma, Y.; Wang, L.; Qin, J.; Li, Q.; Li, Z. *Chem. Commun.* **2012**, *48*, 9586−9588.

(15) Huang, J.; Sun, N.; Yang, J.; Tang, R.; Li, Q.; Ma, D.; Qin, J.; Li, Z. *J. Mater. Chem.* **2012**, *22*, 12001−12007.

(16) Liu, J.-L.; Zhang, J.-Q.; Tang, Z.-L.; Zhuo, Y.; Chai, Y.-Q.; Yuan, R. *Chem. Sci.* **2019**, *10*, 4497−4501.

(17) Jiang, M.-H.; Li, S.-K.; Zhong, X.; Liang, W.-B.; Chai, Y.-Q.; Zhuo, Y.; Yuan, R. *Anal. Chem.* **2019**, *91*, 3710−3716.

(18) Cui, L.; Yu, S.; Gao, W.; Zhang, X.; Deng, S.; Zhang, C.-y. *ACS Appl. Mater. Interfaces* **2020**, *12*, 7966−7973.

(19) Han, Z.; Yang, Z.; Sun, H.; Xu, Y.; Ma, X.; Shan, D.; Chen, J.; Huo, S.; Zhang, Z.; Du, P.; Lu, X. *Angew. Chem., Int. Ed.* **2019**, *58*, 5915−5919.

(20) Han, Z.; Zhang, Y.; Wu, Y.; Li, Z.; Bai, L.; Huo, S.; Lu, X. *Anal. Chem.* **2019**, *91*, 8676−8682.

(21) Wang, N.; Wang, Z.; Chen, L.; Chen, W.; Quan, Y.; Cheng, Y.; Ju, H. *Chem. Sci.* **2019**, *10*, 6815−6820.

(22) Miao, W. *Chem. Rev.* **2008**, *108*, 2506−2553.

(23) Kwon Lee, S.; Bard, A. J. *Anal. Lett.* **1998**, *31*, 2209−2229.

(24) Lai, R. Y.; Bard, A. J. *J. Phys. Chem. B* **2003**, *107*, 5036−5042.

(25) Li, Y.; Jiang, Z. W.; Xiao, S. Y.; Huang, C. Z.; Li, Y. F. *Anal. Chem.* **2018**, *90*, 12191−12197.

(26) Wang, C.; Han, Q.; Liu, P.; Zhang, G.; Song, L.; Zou, X.; Fu, Y. *ACS Sens.* **2021**, *6*, 252−258.

(27) Song, Y.; Zhang, W.; He, S.; Shang, L.; Ma, R.; Jia, L.; Wang, H. *ACS Appl. Mater. Interfaces* **2019**, *11*, 33676−33683.

(28) Li, Y.; Huang, C. Z.; Li, Y. F. *Anal. Chem.* **2019**, *91*, 9308−9314.

(29) Ju, Y.; Park, H.-J.; Shin, I.-S.; Chung, Y. K.; Kim, J. *Inorg. Chem. Commun.* **2019**, *106*, 86−90.

(30) Yu, K.; Wei, T.; Li, Z.; Li, J.; Wang, Z.; Dai, Z. *J. Am. Chem. Soc.* **2020**, *142*, 21267−21271.

(31) Gong, Q.; Hu, Z.; Deibert, B. J.; Emge, T. J.; Teat, S. J.; Banerjee, D.; Mussman, B.; Rudd, N. D.; Li, J. *J. Am. Chem. Soc.* **2014**, *136*, 16724−16727.

(32) Wei, Z.; Gu, Z.-Y.; Arvapally, R. K.; Chen, Y.-P.; McDougald, R. N.; Ivy, J. F.; Yakovenko, A. A.; Feng, D.; Omary, M. A.; Zhou, H.-C. *J. Am. Chem. Soc.* **2014**, *136*, 8269−8276.

(33) Shustova, N. B.; McCarthy, B. D.; Dincă, M. *J. Am. Chem. Soc.* **2011**, *133*, 20126−20129.

(34) Wang, Y.; Zhao, G.; Chi, H.; Yang, S.; Niu, Q.; Wu, D.; Cao, W.; Li, T.; Ma, H.; Wei, Q. *J. Am. Chem. Soc.* **2021**, *143*, 504−512.

(35) Wang, Z.; Jiang, X.; Yuan, R.; Chai, Y. *Biosens. Bioelectron.* **2018**, *121*, 250−256.

(36) Liu, H.; Liu, Z.; Yi, J.; Ma, D.; Xia, F.; Tian, D.; Zhou, C. *Sens. Actuators, B* **2021**, *331*, 129412.

(37) Zhu, D.; Zhang, Y.; Bao, S.; Wang, N.; Yu, S.; Luo, R.; Ma, J.; Ju, H.; Lei, J. *J. Am. Chem. Soc.* **2021**, *143*, 3049−3053.

(38) Janiak, C.; Vieth, J. K. *New J. Chem.* **2010**, *34*, 2366−2388.

(39) Huang, W.; Hu, G.-B.; Yao, L.-Y.; Yang, Y.; Liang, W.-B.; Yuan, R.; Xiao, D.-R. *Anal. Chem.* **2020**, *92*, 3380−3387.

(40) Yang, Y.; Hu, G.-B.; Liang, W.-B.; Yao, L.-Y.; Huang, W.; Zhang, Y.-J.; Zhang, J.-L.; Wang, J.-M.; Yuan, R.; Xiao, D.-R. *Nanoscale* **2020**, *12*, 5932−5941.

(41) Cao, P.; Wang, L.; Cheng, Q.; Sun, X.; Kang, Q.; Dai, L.; Zhou, X.; Song, Z. *Psychiatr. Res.* **2019**, *274*, 189−194.

(42) Wilczynski, M.; Kielbik, M.; Senderowska, D.; Krawczyk, T.; Szymanska, B.; Klink, M.; Bieńkiewicz, J.; Romanowicz, H.; Frühauf, F.; Malinowski, A. *Cancers* **2020**, *12*, 2680.

(43) Sarma, N. J.; Tiriveedhi, V.; Crippin, J. S.; Chapman, W. C.; Mohanakumar, T.; Williams, B. *J. Virol.* **2014**, *88*, 3733−3743.

(44) Wu, X.-H.; Luo, P.; Wei, Z.; Li, Y.-Y.; Huang, R.-W.; Dong, X.-Y.; Li, K.; Zang, S.-Q.; Tang, B. Z. *Adv. Sci.* **2019**, *6*, 1801304.

(45) Li, Y.; He, L.; Huang, C. Z.; Li, Y. F. *Biosens. Bioelectron.* **2019**, *134*, 29−35.

(46) Zhu, M.; Chen, P.; Ma, W.; Lei, B.; Liu, M. *ACS Appl. Mater. Interfaces* **2012**, *4*, 6386−6392.

(47) Li, P.; Bao, Z.; Wang, G.; Xu, P.; Wang, X.; Liu, Z.; Guo, Y.; Deng, J.; Zhang, W. *J. Hazard. Mater.* **2019**, *362*, 336−347.
(48) Liu, L.; Deng, J.; Niu, T.; Zheng, G.; Zhang, P.; Jin, Y.; Jiao, Z.; Sun, X. *J. Colloid Interface Sci.* **2017**, *493*, 281−287.
(49) Xiao, H.; Wang, W.; Pi, S.; Cheng, Y.; Xie, Q. *Anal. Chim. Acta* **2020**, *1135*, 20−28.
(50) Sheng, Z.-H.; Shao, L.; Chen, J.-J.; Bao, W.-J.; Wang, F.-B.; Xia, X.-H. *ACS Nano* **2011**, *5*, 4350−4358.
(51) Gao, T.-B.; Zhang, J.-J.; Yan, R.-Q.; Cao, D.-K.; Jiang, D.; Ye, D. *Inorg. Chem.* **2018**, *57*, 4310−4316.
(52) Lei, Y.-M.; Wen, R.-X.; Zhou, J.; Chai, Y.-Q.; Yuan, R.; Zhuo, Y. *Anal. Chem.* **2018**, *90*, 6851−6858.

https://doi.org/10.1021/acs.analchem.1c04368
Anal. Chem. 2022, 94, 1178−1186